Published in final edited form as:
Biochemistry. 2013 October 8; 52(40): . doi:10.1021/bi400674h.

Computational prediction and *in vitro* analysis of potential physiological ligands of the bile acid binding site in cytochrome *c* oxidase†

Leann Buhrow, **Carrie Hiser**, **Jeffrey R. Van Voorst**¶, **Shelagh Ferguson-Miller***, and **Leslie A. Kuhn**¶,*

Department of Biochemistry and Molecular Biology, Michigan State University, East Lansing, Michigan 48824, United States

¶Department of Computer Science & Engineering, Michigan State University, East Lansing, Michigan 48824, United States

Abstract

A conserved bile acid site has been crystallographically defined in the membrane domain of mammalian and *Rhodobacter sphaeroides* cytochrome *c* oxidase (*Rs*C*c*O). Diverse amphipathic ligands were shown previously to bind to this site and affect the electron transfer equilibrium between heme *a* and a_3 cofactors by blocking the K proton uptake path. Current studies identify physiologically relevant ligands for the bile acid site using a novel three-pronged computational approach: *ROCS* comparison of ligand shape and electrostatics, *SimSite3D* comparison of ligand binding site features, and *SLIDE* screening of potential ligands by docking. Identified candidate ligands include steroids, nicotinamides, flavins, nucleotides, retinoic acid, and thyroid hormones, which are predicted to make key protein contacts with the residues involved in bile acid binding. *In vitro* oxygen consumption and ligand competition assays on *Rs*C*c*O wildtype and its Glu101Ala mutant support regulatory activity and specificity of some of these ligands. An ATP analog and GDP inhibit *Rs*C*c*O under low substrate conditions, while fusidic acid, cholesteryl hemisuccinate, retinoic acid, and T3 thyroid hormone are more potent inhibitors under both high and low substrate conditions. The sigmoidal kinetics of *Rs*C*c*O inhibition in the presence of certain nucleotides is reminiscent of previously reported ATP inhibition of mammalian C*c*O, suggesting regulation involving the conserved core subunits of both mammalian and bacterial oxidases. Ligand binding to the bile acid site is non-competitive with respect to cytochrome *c* and appears to arrest C*c*O in a semi-oxidized state with some resemblance to the “resting” state of the enzyme.

Cytochrome *c* oxidase (C*c*O) is the fourth complex of the electron transport chain responsible for reducing molecular oxygen to water and coupling this reaction to proton pumping.[1,2] C*c*O accepts electrons from cytochrome *c* and sequentially reduces its bimetallic copper A and heme *a* redox centers and finally reduces the binuclear active site

†This work was supported by NIH GM26916 to S.F.-M and includes data with permission from Buhrow, L., Ph.D. dissertation. Computational prediction and experimental validation of cytochrome *c* oxidase main-chain flexibility and allosteric regulation of the K-pathway. Michigan State University, United States – Michigan. (Publication No. AAT 3549123).

*Author for correspondence: Shelagh Ferguson-Miller, 603 Wilson Rd. room 310, Michigan State University, East Lansing, MI 48824 USA, Tel.: 001 517 355 0199, fergus20@msu.edu. *Author for correspondence: Leslie A. Kuhn, 603 Wilson Rd. room 502C, Michigan State University, East Lansing, MI 48824 USA, Tel.: 001 517 353 8745, Fax: 001 517 353 9334, KuhnL@msu.edu, Web: http://www.kuhnlab.bmb.msu.edu.

Supporting Information Available

Complete *ROCS* ligand comparison, *SimSite3D* binding site comparison, and kinetic fitting results may be found in the supporting information. Two-dimensional representations of resultant ligands are also included. This material is free of charge via the Internet at http://pubs.acs.org.

composed of heme a_3 and copper B (Figure 1). Two conserved proton paths, the D- and K-paths, have been identified in bacterial and mammalian oxidases. The K-path takes up one to two protons during active site reduction, while the D-path takes up all other protons consumed during oxygen reduction or pumped across the membrane.[3–5] A bifurcated oxygen channel leading from the membrane environment to the binuclear active site has been crystallographically defined.[6,7] A clear proton exit path has yet to be identified but may involve the heme propionate groups, propionate-associated water molecules, and/or a pair of arginines: Arg481 and Arg482 (*Rhodobacter sphaeroides* numbering is used unless otherwise noted.).[8–13]

C*c*O is thought to be a key regulator of oxidative phosphorylation rate and efficiency.[14–16] In eukaryotic systems, C*c*O activity is modulated by the presence of alternative isoforms of nuclear-encoded accessory subunits,[17–22] phosphorylation at as many as 14 residues including three residues on the conserved enzyme core,[23,24] and binding of small molecules.[25–29] A crystallographically-defined small molecule site with a bound bile acid ligand (Figure 1) has been identified on both bacterial and mammalian C*c*O. This site is located in the membrane interface of subunits I and II, near the entrance to the K-path.[30,31] It has been hypothesized to natively bind nucleotides based on shape, chemistry, and binding preference similarities between ADP and bile acids;[30] however, no structural evidence of nucleotide binding has been obtained.

R. sphaeroides C*c*O (*Rs*C*c*O) has been established as a useful model system to investigate the activity and regulation of mammalian C*c*O.[32] It is suitable for characterizing the bile acid site, as both bovine and *Rhodobacter* oxidases bind bile acids in the same region involving homologous amino acid residues.[30,31,33] *Rs*C*c*O and its K-path mutant form, E101A, are activated or inhibited by a diverse group of ligands that appear to bind at the bile acid site, including detergents, fatty acids, steroids, and porphyrins.[33,34] *Rs*C*c*O inhibition by these ligands and by mutations in the K-path has been attributed to an altered electron transfer equilibrium between heme *a* and a_3 cofactors.[33,35–37] However, the native regulatory ligands for this conserved site remain elusive.

In order to understand the regulation of C*c*O at the bile acid site, a three-pronged computational approach was applied in this work to predict natural ligands with high complementarity to this conserved location. Initially, ligand comparisons were performed using the *ROCS* method[38–39] to identify candidate molecules that are structurally and chemically similar to the crystallographically bound bile acid. Secondly, protein comparisons and alignments were performed using the *SimSite3D* method[40] to search for binding sites that have similar shape and chemistry to the *Rs*C*c*O bile acid site. The native ligands bound to these similar sites were then investigated for their interaction with the bile acid site. Finally, high ranking ligand candidates from both the *ROCS* and *SimSite3D* approaches were docked using *SLIDE*[41–42] to evaluate protein-ligand interactions. All commercially available, soluble, high scoring candidate ligands were tested for their ability to alter the rate of *Rs*C*c*O oxygen consumption. Of these ligand candidates, a cholesterol mimic, a thyroid hormone, retinoic acid, and select nucleotides inhibit *Rs*C*c*O activity. Ligand competition and mutational studies support the binding of these ligands to the bile acid site. Our studies suggest that this region may be polyspecific for a number of native regulatory ligands that arrest C*c*O activity by stabilizing an oxidized binuclear center. This semi-oxidized state has some resemblance to the “resting” state of the bovine enzyme and may have a lesser tendency for oxygen radical byproduct formation.

Materials and Methods

Ligand database selection and processing

The Binding Mother of All Databases (Binding MOAD) [43] is a collection of thousands of crystallographic protein-ligand, protein-cofactor, and protein-ligand-cofactor complexes at or below 2.5 Å resolution. Binding MOAD includes physiologically relevant small molecules except for catalytic molecules (e.g., active site metals, hemes, porphyrins, etc.), covalently bound ligands, crystallographic additives (e.g., buffers, detergents, ions, etc.), and other macromolecules, defined as peptides longer than ten amino acids and DNA fragments larger than four nucleic acid residues. The redundant Binding MOAD database contains multiple copies of proteins with > 90 % sequence identity bound to different molecules and was used to maintain ligand diversity. Identical protein-ligand complexes were manually removed after analysis. This database was selected to assess molecules that complement the *Rs*C*c*O bile acid site, as most of its molecules are natural compounds or analogs of natural compounds rather than synthetic molecules. However, this database is disadvantageous in that it does not contain porphyrin molecules, which have been shown to regulate *Rs*C*c*O activity *in vitro*.[33]

Geometric and chemical comparison of the RsCcO bound deoxycholate to diverse small molecules

*R*apid *O*verlay of *C*hemical *S*tructures (*ROCS* version 2.4.2; OpenEye Scientific Software, Santa Fe, NM) aligns a database of molecules or molecular conformations to a reference ligand structure based on maximizing shape and chemical similarity.[38–39] Ligands are represented by a Gaussian atomic density function about each atom center[38] and aligned such that they have maximal overlap, calculated as in Grant *et al.*, 1996.[39] This overlap is assessed by a Tanimoto or Tversky scoring metric, based on whether overall or substructure matching is desirable. Tanimoto scores, a variation of the Jaccard index, describe the correlation between vectors with continuous or binary attributes representing molecular shape and chemistry. The geometric (ShapeTanimoto) and chemical (ColorTanimoto) similarities are independently scored and scaled between zero and one,[38] resulting in a maximum combined score (TanimotoCombo) of two for exact ligand matches.

ROCS was applied to identify physiological ligands similar in shape or electrostatics to deoxycholate (DOC). The *Rs*C*c*O's bound DOC (Protein Data Bank (PDB): 3DTU[31]) was compared to the crystallographic ligands in Binding MOAD and all low energy conformers of these ligands, as determined by *Omega* version 2.4.2 (OpenEye Scientific Software, Santa Fe, NM).[44] TanimotoCombo score was used to rank the resultant ligand conformations, equally weighing shape and chemical complementarity. All ligands scoring three standard deviations or greater than the average *ROCS* TanimotoCombo score across the entire Binding MOAD database were grouped into dominant chemical classes (e.g., bile acids, steroids, etc.) with redundant ligands removed. Ligands were selected for testing based on TanimotoCombo score ranking, commercial availability, and ability to be solubilized at a concentration sufficient for assaying (≥ 100 μM).

Chemical and shape comparisons of the RsCcO bile acid site and diverse crystallographic sites

The second method used to assess candidate ligands, *SimSite3D*, is a protein binding site alignment and comparison tool that identifies a ranked list of sites most similar to the site of interest. Each site is represented using a set of pharmacophore points with associated bonding geometry and an accompanying solvent accessible molecular surface representing the detailed shape of the site.[40] The pharmacophore points denote positions where non-hydrogen atoms, of the appropriate chemistry, may be placed to form favorable polar or

hydrophobic interactions with atoms in the protein. Polar pharmacophore points have an associated optimal hydrogen-bond direction, used to scale the energy estimate of the hydrogen bond according to its degree of linearity, while the molecular surface matching term ensures that highly ranked sites will have a shape very similar to that of the site of interest.[40]

The *Rs*C*c*O bile acid site was defined about the DOC crystallographic ligand (PDB: 3DTU).[31] The *SimSite3D* default protocol for template generation was used and included all pharmacophore points within 3.0 Å of at least one non-hydrogen atom of DOC. The molecular surface of the site, within 4.0 Å of DOC, was computed using the MSMS method.[45] Binding MOAD sites' pharmacophore points were optimally aligned to the pharmacophore points of the *Rs*C*c*O bile acid site by *SimSite3D* into the *Rs*C*c*O frame of reference. All ligand sites found in Binding MOAD were ranked based on *SimSite3D* score, calculated as

$$SimSite\,\text{score} = -2.62899 - 0.0122689\,\alpha - 0.00619202\,\beta + 2.11849\,\gamma$$

where α is the sum of the number of matched hydrogen bond donor and hydrogen bond acceptor groups, β is the sum of matched chemical groups that may serve as either hydrogen bond donor or acceptor groups, and γ is the root mean standard error between aligned surfaces which also reflects hydrophobic surface matching.[40] Of the thousands of protein sites from Binding MOAD analyzed by *SimSite3D*, those sites scoring two standard deviations greater than the average *SimSite3D* score across Binding MOAD were analyzed as the best candidates for being physiologically relevant. These sites were grouped into dominant chemical classes (e.g., steroid, nucleotide, or lipid binding proteins), with redundant protein-ligand crystallographic complexes removed.

Small molecule docking of predicted ligands into the RsCcO bile acid site

In the third approach to identify physiological ligand candidates, the *Rs*C*c*O bile acid site with bound DOC removed (PDB: 3DTU)[31] was used as the target for *SLIDE* (*S*creening *L*igands by *I*nduced-fit *D*ocking, *E*fficiently)[41–42] prediction of the binding modes of *ROCS* and *SimSite3D* candidate ligands. Similar to the *SimSite3D* representation, *SLIDE* characterizes favorable positions for protein-ligand hydrophobic interactions or hydrogen bonds in a binding pocket by generating a template of chemistry-labeled points. To fully sample candidate ligand flexibility, *Omega* version 2.4.2 was used to generate all low-energy conformations of the ligands prior to docking. *SLIDE* predicts the ligand binding orientation for each molecule by first sampling all matches between triplets of ligand atoms with complementary chemical type and interatomic distance to triplets of protein template points, resulting in alternative dockings that exhibit shape and chemical complementarity between the protein and ligand. The best orientation is then chosen according to the most favorable $\Delta G_{binding}$ value according to *SLIDE*'s OrientScore [Tonero, Zavodszky, Van Voorst, He, Arora, Namilikonda, and Kuhn, *in preparation*]. *SLIDE*'s AffiScore then ranks the ligand candidates by a more detailed weighted sum of favorable hydrophobic and hydrogen-bonding interaction terms and unfavorable (unsatisfied/repulsive) interaction terms between the protein and docked ligand to assess their relative $\Delta G_{binding}$. Additionally, the dominant interactions between the diverse docked ligands and the *Rs*C*c*O bile acid site were tabulated according to frequently contacted protein residues.

RsCcO purification and oxygen consumption activity assays

R. sphaeroides strains overexpressing the 37-2 wild-type (WT) C*c*O[46] and E101A mutant[47] were grown as previously described. Cell membranes were prepared and *Rs*C*c*O was isolated by metal affinity chromatography as described for crystallographic studies.[47] Oxygen uptake rates were measured with a Clark-type electrode, and turnover rates (TN in electrons per second per C*c*O molecule) were calculated as described in Hosler *et al.*, 1992.[32] Assay mixtures contained 100 mM HEPES pH 7.4, 24 mM KCl, 2.8 mM ascorbate, 1 mM N,N,N′,N′-tetramethyl-p-phenylenediamine (TMPD), 5.6 μM EDTA, 0.01% lauryl maltoside (LM), with 0–30 μM purified bovine heart cytochrome *c* as the substrate and other additives as noted. Farnesyl diphosphate was purchased from Echelon Biosciences Incorporated (Logan, UT). All other additives were from Sigma-Aldrich (St. Louis, MO). Cholesteryl hemisuccinate and mammalian steroid hormones were dissolved in ethanol, retinoic acid was dissolved in DMSO, T3 thyroid hormone was dissolved in 0.1 N NaOH, and all other ligands were dissolved in water. Ligand effects were determined by the change in activity compared to an equal volume of the solvent alone. Prism version 6 (Graphpad Software, La Jolla, CA) was used to calculate kinetic values. Ligand titrations were fit with allosteric sigmoidal least-squares regression, and IC50 values were reported. Cytochrome *c* titrations were fit with the mixed inhibition model, a general form of non-competitive inhibition, with least-squares regression and reported K_i values.

Results

Chemical and geometric comparisons between the CcO crystallographic deoxycholate and diverse ligands

Mammalian and bacterial C*c*O proteins have been crystallized in the presence of bile acids, cholate in the case of bovine C*c*O (bovC*c*O)[30] and DOC in the case of *Rs*C*c*O.[31] The ability of bile acids to bind to a conserved site and inhibit activity invokes the hypothesis that they mimic structurally similar, native regulatory molecules. In order to understand which potential physiological ligands are significantly similar to the bound DOC, the *ROCS* method was used to evaluate chemical and geometric similarities between DOC and ligands in the Binding MOAD database. Six chemical classes of ligands were identified, including bile acids, steroids, retinoic acid analogs, amino acid analogs, nucleotide and flavin analogs, and thyroid hormone analogs (Table 1 and Supplemental Table 1). *ROCS* alignments of these predicted ligands to the crystallographic DOC resulted in an overlay of polycyclic ligand groups with the DOC steroid ring system and aliphatic, carboxylate, or phosphorylated ligand tails with the DOC carboxylate tail (Figure 2 and Supplemental Figure 1). It had been suggested previously that the bile acid site is in fact an allosteric regulatory site that binds ADP under physiological conditions.[30] The similarity between DOC and abundant adenine-containing ligands and nucleotides was also evaluated by *ROCS* with thirteen nucleotides, FAD, and a NAD^+ analog scoring highly structurally and chemically similar to DOC (Supplemental Table 2).

Chemical and geometric comparisons between the CcO bile acid site and diverse protein sites

In order to predict varied candidate ligands that complement *Rs*C*c*O, rather than just those similar to DOC, the C*c*O bile acid binding site was compared to diverse ligand sites in Binding MOAD using the *SimSite3D* method. *SimSite3D* compares crystallographic protein sites based on surface chemistry and geometry, using no knowledge of the existing bound ligand or the underlying amino acid sequence.[40] This approach identified five classes of protein sites, characterized by their bound flavin, lipid, nicotinamide, nucleotide, and steroid ligands (Table 1 and Supplemental Table 3). Interestingly, no bile acid binding proteins were identified as high scoring by *SimSite3D*. Striking overlap between the *ROCS* and

SimSite3D ligand candidates is observed as both methods identified hydrocortisone, cholesterol, aldosterone, FAD, NAD^+, GDP, ATP, and ADP, despite *ROCS* only using DOC ligand information and *SimSite3D* only using knowledge of the *Rs*C*c*O bile acid site with DOC removed.

Prediction of critical amino acid residues and candidate ligand binding orientations in the CcO bile acid site

The *ROCS* method of ligand comparison and *SimSite3D* method of protein site comparison identified candidate ligands with the potential to affect C*c*O by specifically interacting at the bile acid site. However, neither of these results provided information about the interactions between the candidate ligands and the amino acid side chains of the C*c*O bile acid site. To understand the binding orientation and relative energetic favorability of candidate molecules, these ligands were docked into the *Rs*C*c*O bile acid site with *SLIDE*. The docked ligands interacted with eight residues: P315 and Y318 in subunit I and H96, S98, E101, I102, W104, and T105 in subunit II (Table 2). Additionally, the diverse protein sites aligned to *Rs*C*c*O by *SimSite3D* indicate five residues, based on aligned chemical groups, are responsible for the dominant chemical interactions in the bile acid site. These residues are P315 in subunit I and H96, S98, E101, and T105 in subunit II (Figure 3). The consensus between *SLIDE* docking and *SimSite3D* alignment of five amino acids supports the role of these residues in ligand binding and will guide mutagenesis efforts in subsequent work.

In addition to the identification of five consensus residues in the bile acid site, *SimSite3D* alignment suggests variation in hydrophobic and hydrophilic ligand binding. The *SimSite3D* protein site classes that bound flavin, nicotinamide, or nucleotide ligands contained chemical groups analogous to the five dominant residues in the bile acid site (Table 3). Lipidic or steroidal ligand binding sites, from the mostly soluble proteins in Binding MOAD, were less similar to the bile acid site, as these sites matched fewer C*c*O residues. These results suggest that either this site may be more complementary to hydrophilic ligands despite its location in the membrane domain or that the BindingMOAD database entries from the PDB, containing mostly soluble proteins, have insufficient examples of hydrophobic ligand binding sites for a comprehensive comparison. Nevertheless, hydrophobic and amphipathic ligands have the strongest effect on *Rs*C*c*O activity under the *in vitro* assay conditions used (in this work and Hiser *et al.*, 2013[33]). The results raise the possibility that the C*c*O bile acid site may interact with hydrophobic ligands such as lipids or steroids more strongly when in contact with the membrane/detergent environment, but may change in affinity and specificity toward hydrophilic ligands when the membrane environment is interrupted by protein/protein interactions upon formation of dimers and higher molecular weight complexes.[30,48]

Interestingly, both the *SimSite3D* protein site comparison and *SLIDE* docking methods identified similar binding orientations among the analyzed riboside ligands (Figure 4). By optimally aligning protein sites with *SimSite3D* and including the crystallographic bound ligands in the same reference frame, the approximate ligand binding orientations can be inferred and compared to ligand dockings. Riboside ligands interacted with the *Rs*C*c*O bile acid site via 1) the ligand phosphate groups with H96 and E101, 2) the ligand ribose with T105, and 3) the ligand nitrogenous base or other cyclic group with the P315 hydrophobic pocket. The identification of similar binding orientations using two independent methods and between structurally similar ligands suggests there are conserved features of ADP, ATP, GDP, FAD, and NAD^+ binding in the C*c*O steroid binding site.

In vitro assay of CcO regulation by the candidate ligands

ROCS ligand comparisons and *SimSite3D* protein site comparisons identified an overlapping but diverse set of candidate ligands (Table 1). To assess the ability of high scoring,

commercially available ligands to act as regulators, the oxygen consumption activity of *Rs*C*c*O was monitored at saturating cytochrome *c* concentrations in the presence and absence of individual candidate ligands (Figure 5). An ATP analog [adenosine 5′-(β, γ-imido) triphosphate] and GDP were assayed at physiological millimolar concentrations,[49] similar to those previously observed to regulate mammalian C*c*O *in vitro*.[25–27,50–51] Both ligands inhibited activity of *Rs*C*c*O under saturating cytochrome *c* concentrations to a similar limited extent (Figure 5A) with similar affinities (Figure 5B), as assessed by the half maximal inhibitory concentration for the ATP analog (IC50 = 4.4 mM) and GDP (IC50 = 4.6 mM). Fusidic acid (IC50 = 3.4 mM), cholesteryl hemisuccinate (CHS; IC50 = 240 μM), retinoic acid (IC50 = 1.7 mM), and T3 thyroid hormone (IC50 = 210 μM) are more potent inhibitors, some in the micromolar range. Other predicted ligands including ADP, FAD, farnesyl diphosphate, NAD^+ (Figure 5A), and the hydrophobic steroids testosterone, estradiol, hydrocortisone, and aldosterone (Supplemental Figure 2) had no significant effect.

Retinoic acid, fusidic acid, and the ATP analog elicited a biphasic response: activation at low ligand concentration followed by inhibition at higher concentration (Figure 5B). This behavior has been observed previously upon addition of amphipathic ligands to the *Rs*C*c*O mutant, E101A, under standard assay conditions (0.06% LM) and to WT in 0.01% detergent (Figure 6). This initial activation effect in E101A has been attributed to chemical rescue by carboxyl group replacement and the displacement of inhibitory detergent, while the subsequent inhibition is hypothesized to result from a ligand-specific effect.[33] Detergent sensitivity of the larger, more hydrophobic bile acid site in the E101A mutant, but not in the WT, has been demonstrated.[33] Additionally, detergent sensitivity to biphasic ligand-induced effects is only observed in the E101A mutant and not in the WT enzyme.[52] These results suggest that biphasic effects of ligands binding to the WT enzyme are due to more than one interaction mode, activating at low concentrations and inhibiting at high concentrations, independently of detergent. Yet these biphasic effects are associated with the bile acid region since both are altered by the E101A mutation (Figure 6 and see below). Clearer understanding of this complex activation/inhibition behavior awaits further structural and mutagenic studies.

Mutation and ligand competition analyses support binding to the bile acid site

The three-pronged computational approach was applied to identify biological ligands that may regulate C*c*O at the bile acid site. To test the binding location of the C*c*O inhibitors predicted in this work, a form of the *Rs*C*c*O with a mutation in one of the five consensus bile acid residues (Table 2 and Figure 3), E101A, was monitored for ligand-induced activity changes. In addition to E101 being identified as a key residue by both *SimSite3D* and *SLIDE*, its mutant form has been shown to be a sensitive system for investigating ligand binding to the bile acid site.[33] When assayed with the E101A mutant, the ATP analog and GDP showed very low stimulation and no inhibition of activity.[52] The cholesterol mimic CHS (IC50 = 530 μM) still inhibited the mutant but with reduced affinity (Figure 6). These lower binding affinities are consistent with the predicted dominant role of E101 in hydrophilic ligand binding to the bile acid site (Tables 2 and 3). In contrast, both retinoic acid (IC50 = 190 μM) and T3 thyroid hormone (IC50 = 66 μM) appeared to bind more tightly to the mutant, as might be expected based on the predicted lesser dependence of lipidic ligands on E101 (Table 3) and the increased overall hydrophobicity of the site. In all cases, the mutation had a significant influence on the ligand behavior, consistent with the predicted characteristics of the bile acid site.

To further test the localization of nucleotide binding to the bile acid site, the ability of the crystallographically-observed DOC ligand to inhibit *Rs*C*c*O activity was monitored in the presence and absence of the ATP analog. DOC is a stronger inhibitor (IC50 = 1.4 mM) than

the ATP analog (IC50 = 4.4 mM) and can lower *Rs*CcO activity by more than 90% (Figure 7). At 5 mM concentration, the ATP analog alone elicits no effect as this is the mid-point of the ligand's biphasic affect (Figure 5B). However, at this concentration, the ATP analog prevented DOC in the 0–2 mM range from inhibiting *Rs*CcO activity, showing its ability to compete with the bile acid (Figure 7). Together, the DOC competition and the effects of the E101A mutation support the prediction that nucleotides bind at the bile acid site and that both their initial activation and subsequent inhibition of C*c*O is mediated by this region.

Non-saturating cytochrome c concentrations reveal sigmoidal and non-competitive patterns of inhibition

The regulation of mammalian C*c*O by nucleotides and thyroid hormone has been observed previously by investigating ligand effects at a range of non-saturating to saturating levels of cytochrome *c*.[25–27,50,51] As the present work has discovered nucleotide effects on bacterial C*c*O, all candidate ligands were further tested for their ability to influence *Rs*C*c*O activity at non-saturating cytochrome *c* concentrations. Fusidic acid (K_i = 2.5 mM), CHS (K_i = 290 μM), retinoic acid (K_i = 140 μM), and T3 thyroid hormone (K_i = 30 μM) were observed to be strong inhibitors at all substrate concentrations (Figure 8A; Supplemental Table 4), while NAD^+ (Figure 8A) and the hydrophobic steroids testosterone, estradiol, hydrocortisone, and aldosterone (data not shown) failed to affect *Rs*C*c*O under low or high concentrations of cytochrome *c*. In contrast, physiological concentrations of ADP (K_i = 3.1 mM), the ATP analog (K_i = 1.5 mM), and GDP (K_i = 1.7 mM) inhibited *Rs*C*c*O most strongly at cytochrome *c* concentrations below 15 μM (Figure 8B; Supplemental Table 4). The effects of these ligands were fit with noncompetitive inhibition, selected as its regression better described the activity with non-saturating cytochrome *c* levels, compared to competitive inhibition models.

Under these assay conditions, *Rs*C*c*O inhibition by nucleotides gives rise to a sigmoidal curve (Figure 8B), similar to the behavior observed in mammalian C*c*O in the presence of ATP.[25–27,50,51] Originally, this sigmoidal inhibition of bovC*c*O was argued to represent negative cooperativity between cytochrome *c* substrate binding sites on the mammalian dimer elicited by ATP binding on the matrix domains of nuclear-encoded subunits IV or VI.[26,27] Allosteric regulation of bacterial C*c*O by nucleotides had not been observed prior to this study. This lack of inhibition was suggested to be due to the absence of nuclear-encoded subunits containing the ATP regulatory sites.[53] However, the sigmoidal curves observed in non-saturating cytochrome *c* assays of *Rs*C*c*O in the presence of nucleotides suggests that this inhibitory effect must be due to ligand binding on the core subunits of the C*c*O, potentially at the bile acid site.

DOC inhibition of the *Rs*C*c*O WT and the E101A mutant (Figure 9) is also consistent with noncompetitive inhibition with respect to cytochrome *c*, characterized by an altered V_{max} but no change in apparent K_m for cytochrome *c*. Additionally, the T3 thyroid hormone noncompetitively inhibits the *Rs*C*c*O WT (data not shown). These results suggest that C*c*O inhibition by ligand binding to the bile acid site, including the sigmoidal inhibition by nucleotides, is unlikely to be explained by allosterically altered cytochrome *c* affinity. An alternative model consistent with the kinetic, crystallographic[33] and spectral studies[33,35–37] is preferential ligand binding to the oxidized form of the enzyme, affecting K-path proton uptake (see Discussion).

Discussion

C*c*O regulates cell metabolism and oxidative phosphorylation efficiency.[14–16] Its function is also controlled through highly regulated expression and assembly[14–16] and tissue specific isoforms.[17] Eukaryotic C*c*O is subject to phosphorylation of at least fourteen characterized

sites, including three sites on the subunit I-III core.[23] In addition, regulation by adenine nucleotides[25–27,50,51,53] and other small molecules[25,33,54–57] has been reported. The structural and mechanistic basis of these observed regulatory processes is difficult to investigate in the complex mammalian enzyme. However, the simpler bacterial model system has permitted computational, mutagenic, and functional analyses to characterize small molecule regulation at a conserved bile acid binding site.[33,34]

Physiological relevance of identified CcO inhibitors

This work's three-pronged computational approach has identified five candidate ligands that affect C*c*O activity and have previously been tied to metabolic regulation. Thyroid hormones, including T3, have been shown to stimulate metabolism,[58] to interact specifically with intact mitochondria,[54,59,60] and to alter C*c*O activity.[61,62] Retinoic acid, the degradative product of the essential vitamin A, has been tied to mitochondrial functions including transcriptional regulation, thermogenesis, and apoptosis.[63,64] High ratios of ATP / ADP, but not other nucleotides[50], have been shown to inhibit mammalian C*c*O.[25,26,51] Additionally, fusidic acid, a porphyrin-binding mimic,[65] has been identified as a C*c*O inhibitor. It is important to note that porphyrin molecules are not present in the Binding MOAD database and were therefore not evaluated by *ROCS* or *SimSite3D*. However, protoporphyrin IX and bilirubin have been previously shown to strongly interact with the C*c*O bile acid site and affect activity.[33] One interpretation of these results is that the conserved bile acid site is a polyspecific regulatory site whose ligands may include ATP, GDP, steroids, retinoic acid, T3 thyroid hormone, and porphyrins. This site may then regulate oxidative phosphorylation based on local energetic demand using a varied set of ligands, whose abundance, affinity and effects will depend on the tissue, the nuclear-encoded subunit isoform and the metabolic state. It is interesting to note that bovC*c*O subunit VIa impacts directly on the bile acid binding site[30] and could modify the binding site's specificity through subunit phosphorylation.[23,24] In addition, the location of the bile acid site in bovC*c*O is at the crystallographic dimer interface and in proximity to a cardiolipin site, raising further possibilities of variable ligand specificity and regulatory influence on supercomplex formation.[48]

Ligand binding to the CcO bile acid site may arrest the protein's active site in an oxidized state

Previous work concluded that the nature of the regulatory effect of bile acid site ligands involved inhibition of the K proton uptake path.[33] In the fully active enzyme starting from the oxidized state, transfer of the first two electrons from cytochrome *c* results in a reduced active site (heme a_3 $^{2+}$/Cu_B $^{1+}$) which can then bind oxygen and proceed with catalysis of oxygen reduction.[3,66] In contrast, inhibition of the K-path favors retention of electrons by heme *a* and Cu_A such that the active site is not reduced and has low affinity for oxygen.[33,35–37] This inhibited state is observed spectrally as an increased steady-state ratio of reduced heme *a* to reduced heme a_3 upon ligand binding to the bile acid site or mutation of K-path residues.[33,36,37] The simplest interpretation of these observations is a direct block of K-path-dependent reduction of heme a_3. If, instead, ligand binding allosterically inhibited the D proton uptake path, irreversible suicide inactivation would be expected.[67,68] However, this phenomenon is not observed. Therefore, by regulating C*c*O through the K-path, enzyme activity can be controlled transiently in response to changing physiological conditions without altering the enzyme's integrity.

Two hypotheses have been proposed for the mechanism of K-path inhibition.[33] Firstly, mutations and ligand binding to the bile acid site may disrupt or constrain dynamic water molecules likely required for proton conductance in the K-path.[33,34,69] Indeed, the *Rs*C*c*O crystal structure in the DOC-bound state shows an increased number of well-resolved, stable

water molecules in the K-path entry.[31] Secondly, mutations and ligand binding may restrict conformational change of subunit I helix VIII,[33] which has been shown to be flexible by crystallography,[70] solvent accessibility,[71] and intrinsic flexibility calculations.[72] The latter hypothesis is further supported by crystallographic studies indicating preferential binding of DOC to the oxidized form[33] and the sigmoidal kinetics of nucleotide inhibition (Figure 8B), suggesting that at low cytochrome *c* concentrations (hence more oxidized state) the ligands bind with greater affinity.

A plausible rationale for controlling C*c*O via affecting the K-path may be understood by considering the conservation of this path and its role in the catalytic cycle. The K-path is the only proton uptake path conserved in heme/copper oxidases from bacteria to mammals.[73,74] Therefore, the K-path represents both an ancestral and conserved target for regulation. Further, by blocking the K-path, the enzyme is arrested in a semi-oxidized state (Cu_A, heme *a* reduced; Cu_B, heme a_3 oxidized), which has a low affinity for O_2 binding,[66,75,76] lessening the probability of forming damaging reactive oxygen species. Indeed, a form of bovC*c*O with slowed turnover, a similar decreased heme *a* to a_3 electron transfer rate, and an oxidized active site has been previously characterized as the “resting” or “slow” form of C*c*O.[77–82] We suggest that this commonly observed state could represent a form in which a detergent, such as cholate, or other ligand is already occupying the bile acid site. A similar hypothesis was previously proposed[82] with respect to another bile acid binding site that is also at the dimer interface of the bovine enzyme, but is not conserved in the bacterial form. However, unlike the bovC*c*O resting form,[78–82] a spectral shift in the Soret band is not observed in the ligand-inhibited *Rs*C*c*O, [33] and the EPR and cyanide binding characteristics of the inhibited bacterial form have yet to be explored.

Conclusions

Three complementary computational methods have been applied in this study to predict possible physiological ligands for the conserved C*c*O bile acid site. *In vitro* oxygen consumption assays validated an ATP analog, GDP, cholesteryl hemisuccinate, retinoic acid, and T3 thyroid hormone as inhibitors of *Rs*C*c*O. Porphyrin ligands are also implicated based on the prediction of the porphyrin mimic fusidic acid and previous evidence of porphyrin regulation.[33] These ligands were confirmed to interact at or near the bile acid site based on their differential effects on the bile acid binding site mutant, E101A, and competition with the crystallographically-identified ligand, DOC. This work provides an initial characterization of bacterial C*c*O regulation by nucleotides, exhibiting sigmoidal kinetics reminiscent of the ATP inhibition of mammalian C*c*O and ties this regulation to the bile acid site on the enzyme’s core subunits, common to both bacterial and mammalian oxidases.

We propose ligand binding at the bile acid site, which is noncompetitive with respect to cytochrome *c*, affects C*c*O activity by altering the K-path dependent proton uptake. This can result in the arrest of C*c*O in a form resembling a “resting” state, where the active site is oxidized and has little potential for generating oxygen radical byproducts. The location and conservation of the binding site and the regulatory response suggest that small molecule interactions at the bile acid site may be an important mechanism of modulating oxidative phosphorylation.

Supplementary Material

Refer to Web version on PubMed Central for supplementary material.

Acknowledgments

The authors thank OpenEye Scientific Software (Santa Fe, NM) for providing an academic license for the use of *ROCS* and *Omega* software.

List of Abbreviations

bov*Cc*O	Bovine C*c*O
CHS	cholesteryl hemisuccinate
C*c*O	cytochrome *c* oxidase
DOC	deoxycholate
n-dodecyl-β-D-maltoside; LM	lauryl maltoside
***Rs*C*c*O**	*Rhodobacter sphaeroides* C*c*O
TMPD	N,N,N′,N′-tetramethyl-p-phenylenediamine
WT	wild-type

References

1. Hosler JP, Ferguson-Miller S, Mills DA. Energy transduction: Proton transfer through the respiratory complexes. Annu Rev Biochem. 2006; 75:165–187. [PubMed: 16756489]
2. Ferguson-Miller S, Babcock GT. Heme/copper terminal oxidases. Chem Rev. 1996; 96:2889–2908. [PubMed: 11848844]
3. Brändén M, Tomson F, Gennis RB, Brzezinski P. The entry point of the K-proton-transfer pathway in cytochrome *c* oxidase. Biochemistry. 2002; 41:10794–10798. [PubMed: 12196018]
4. Ruitenberg MR, Aimo K, Bamberg E, Fendler K, Michel H. Reduction of cytochrome *c* oxidase by a second electron leads to proton translocation. Nature. 2002; 417:99–102. [PubMed: 11986672]
5. Bloch D, Belevich I, Jasaitis A, Ribacka C, Puustinen A, Verkhovsky MI. The catalytic cycle of cytochrome *c* oxidase is not the sum of its two halves. Proc Natl Acad Sci USA. 2004; 101:529–533. [PubMed: 14699047]
6. Luna VM, Chen Y, Fee JA, Stout CD. Crystallographic studies of Xe and Kr binding within the large internal cavity of cytochrome *ba*3 from *Thermus thermophilus*: Structural analysis and role of oxygen transport channels in the heme–cu oxidases. Biochemistry. 2008; 47:4657–4665. [PubMed: 18376849]
7. Luna VM, Fee JA, Deniz AA, Stout CD. Mobility of Xe atoms within the oxygen diffusion channel of cytochrome *ba*(3) oxidase. Biochemistry. 2012; 51:4669–4676. [PubMed: 22607023]
8. Qian J, Mills DA, Geren L, Wang K, Hoganson CW, Schmidt B, Hiser C, Babcock GT, Durham B, Millett F, Ferguson-Miller S. Role of the conserved arginine pair in proton and electron transfer in cytochrome *c* oxidase. Biochemistry. 2004; 43:5748–5756. [PubMed: 15134449]
9. Mills DA, Geren L, Hiser C, Schmidt B, Durham B, Millett F, Ferguson-Miller S. An arginine to lysine mutation in the vicinity of the heme propionates affects the redox potentials of the hemes and associated electron and proton transfer in cytochrome *c* oxidase. Biochemistry. 2005; 44:10457–10465. [PubMed: 16060654]
10. Seibold SA, Mills DA, Ferguson-Miller S, Cukier RI. Water chain formation and possible proton pumping routes in *Rhodobacter sphaeroides* cytochrome *c* oxidase: A molecular dynamics comparison of the wild type and R481K mutant. Biochemistry. 2005; 44:10475–10485. [PubMed: 16060656]
11. Egawa T, Lee HJ, Gennis RB, Yeh SR, Rousseau DL. Critical structural role of R481 in cytochrome *c* oxidase from *Rhodobacter sphaeroides*. Biochim Biophys Acta. 2009; 1787:1271–1275.
12. Lee HJ, Ojemyr L, Vakkasoglu A, Brzezinski P, Gennis RB. Properties of Arg481 mutants of the *aa*3-type cytochrome *c* oxidase from *Rhodobacter sphaeroides* suggest that neither R481 nor the

nearby D-propionate of heme *a*3 is likely to be the proton loading site of the proton pump. Biochemistry. 2009; 48:7123–7131. [PubMed: 19575527]

13. Popović DM, Stuchebrukhov AA. Proton exit channels in bovine cytochrome *c* oxidase. J Phys Chem B. 2006; 109:1999–2006. [PubMed: 16851184]
14. Pacelli C, Latorre D, Cocco T, Capuano F, Kukat C, Seibel P, Villani G. Tight control of mitochondrial membrane potential by cytochrome *c* oxidase. Mitochondrion. 2011; 11:334–341. [PubMed: 21147274]
15. Villani G, Attardi G. *In vivo* control of respiration by cytochrome *c* oxidase in wild-type and mitochondrial DNA mutation-carrying human cells. Proc Natl Acad Sci USA. 1997; 94:166–1171.
16. Hüttemann M, Helling S, Sanderson TH, Sinkler C, Samaviti L, Mahapatra G, Varughuese A, Lu G, Liu J, Grossman LI, Doan JW, Marcus K, Lee I. Regulation of mitochondrial respiration and apoptosis through cell signaling: Cytochrome *c* oxidase and cytochrome *c* in ischemia/reperfusion injury and inflammation. Biochim Biophys Acta. 2012; 1817:598–609. [PubMed: 21771582]
17. Pierron D, Wildman DE, Hüttemann M, Markondapatnaikuni GC, Aras S, Grossman LI. Cytochrome *c* oxidase: Evolution of control via nuclear subunit addition. Biochim Biophys Acta. 2012; 1817:590–597. [PubMed: 21802404]
18. Das J, Miller ST, Stern DL. Comparison of diverse protein sequences of the nuclear-encoded subunits of cytochrome *c* oxidase suggest conservation of structure underlies evolving functional sites. Mol Biol Evol. 2004; 21:1572–1582. [PubMed: 15155798]
19. LaMarche AEP, Abate MI, Chan SHP, Trumpower BL. Isolation and characterization of *COX12*, the nuclear gene for a previously unrecognized subunit of *Saccharomyces cerevisiae* cytochrome *c* oxidase. J Biol Chem. 1992; 276:22473–22480. [PubMed: 1331057]
20. Hüttemann M, Kadenbach B, Grossman LI. Mammalian subunit IV isoforms of cytochrome *c* oxidase. Gene. 2001; 267:111–123. [PubMed: 11311561]
21. Hüttemann M, Schmidt TR, Grossman LI. A third form of cytochrome *c* oxidase subunit VII is present in mammals. Gene. 2003; 312:95–102. [PubMed: 12909344]
22. Grossman LI, Lomax MI. Nuclear encoded genes for cytochrome *c* oxidase. Biochim Biophys Acta. 1997; 1352:174–192. [PubMed: 9199249]
23. Hüttemann M, Lee I, Grossman LI, Doan JW, Sanderson TH. Phosphorylation of mammalian cytochrome *c* and cytochrome *c* oxidase in the regulation of cell destiny: Respiration, apoptosis, and human disease. Adv Exp Med Biol. 2012; 748:237–264. [PubMed: 22729861]
24. Fang JK, Prabu SK, Sepuri NB, Raza H, Anandatheerthavarada HK, Galati D, Spear J, Avadhani NG. Site specific phosphorylation of cytochrome *c* oxidase subunits I, IVi1, and Vb in rabbit hearts subjected to ischemia/reperfusion. FEBS Lett. 2007; 581:1302–1310. [PubMed: 17349628]
25. Arnold S, Goglia F, Kadenbach B. 3,5-Diiodothyronine binds to subunit Va of cytochrome-*c* oxidase and abolishes the allosteric inhibition of respiration by ATP. Eur J Biochem. 1998; 252:325–330. [PubMed: 9523704]
26. Arnold S, Kadenbach B. Cell respiration is controlled by ATP, an allosteric inhibitor of cytochrome-*c* oxidase. Eur J Biochem. 1997; 249:350–354. [PubMed: 9363790]
27. Bender E, Kadenbach B. The allosteric ATP-inhibition of cytochrome *c* oxidase activity is reversibly switched on by cAMP-dependent phosphorylation. FEBS Lett. 2000; 466:130–134. [PubMed: 10648827]
28. Lee I, Bender E, Kadenbach B. Control of mitochondrial membrane potential and ROS formation by reversible phosphorylation of cytochrome *c* oxidase. Mol Cell Biochem. 2002; 234–235:63–70.
29. Lee I, Salomon AR, Ficarro S, Mathes I, Lottspeich F, Grossman LI, Hüttemann M. cAMP-dependent tyrosine phosphorylation of subunit I inhibits cytochrome *c* oxidase activity. J Biol Chem. 2005; 280:6094–6100. [PubMed: 15557277]
30. Tsukihara T, Aoyama H, Yamashita E, Tomizaki T, Yamaguchi H, Shinzawa-Itoh K, Nakashima R, Yaono R, Yoshikawa S. The whole structure of the 13-subunit oxidized cytochrome *c* oxidase at 2.8 angstrom. Science. 1996; 272:1136–1144. [PubMed: 8638158]
31. Qin L, Mills DA, Buhrow L, Hiser C, Ferguson-Miller S. A conserved steroid binding site in cytochrome *c* oxidase. Biochemistry. 2008; 47:9931–9933. [PubMed: 18759498]
32. Hosler JP, Fetter J, Tecklenburg MMJ, Espe M, Lerma C, Ferguson-Miller S. Cytochrome-*aa*3 of *Rhodobacter sphaeroides* as a model for mitochondrial cytochrome *c* oxidase - Purification,

kinetics, proton pumping, and spectral analysis. J Biol Chem. 1992; 267:24264–24272. [PubMed: 1332949]

33. Hiser C, Buhrow L, Liu J, Kuhn L, Ferguson-Miller S. A conserved amphipathic ligand binding region influences K-path-dependent activity of cytochrome *c* oxidase. Biochemistry. 2013; 52:1385–1396. [PubMed: 23351100]
34. Ferguson-Miller S, Hiser C, Liu J. Gating and regulation of the cytochrome *c* oxidase proton pump. Biochim Biophys Acta. 2012; 1817:489–494. [PubMed: 22172738]
35. Vik SB, Capaldi RA. Lipid requirements for cytochrome-*c* oxidase activity. Biochemistry. 1977; 16:5755–5759. [PubMed: 201276]
36. Konstantinov AA, Siletsky S, Mitchell D, Kaulen A, Gennis RB. The roles of the two proton input channels in cytochrome *c* oxidase from *Rhodobacter sphaeroides* probed by the effects of site-directed mutations on time-resolved electrogenic intraprotein proton transfer. Proc Natl Acad Sci USA. 1997; 94:9085–9090. [PubMed: 9256439]
37. Antalik M, Jancura D, Palmer G, Fabian M. A role for the protein in internal electron transfer to the catalytic center of cytochrome *c* oxidase. Biochemistry. 2005; 44:14881–14889. [PubMed: 16274235]
38. Hawkins PCD, Skillman AG, Nicholls A. Comparison of shape-matching and docking as virtual screening tools. J Med Chem. 2007; 50:74–82. [PubMed: 17201411]
39. Grant JA, Gallardo MA, Pickup BT. A fast method of molecular shape comparison: A simple application of a Gaussian description of molecular shape. J Comput Chem. 1996; 17:1653–1666.
40. Van Voorst, Jeffrey Ryan. PhD thesis. Michigan State University; 2011. Surface matching and chemical scoring to detect unrelated proteins binding similar small molecules; p. 3465552
41. Schnecke V, Swanson CA, Getzoff ED, Tainer JA, Kuhn LA. Screening a peptidyl database for potential ligands to proteins with side-chain flexibility. Proteins. 1998; 33:74–87. [PubMed: 9741846]
42. Zavodszky MI, Sanschagrin PC, Korde RS, Kuhn LA. Distilling the essential features of a protein surface for improving protein-ligand docking, scoring, and virtual screening. J Comput Aid Mol Des. 2002; 16:883–902.
43. Benson ML, Smith RD, Khazanov NA, Dimcheff B, Beaver J, Dresslar P, Nerothin J, Carlson HA. Binding MOAD, a high-quality protein-ligand database. Nucleic Acids Res. 2007; 36:D674–D678. [PubMed: 18055497]
44. Hawkins PCW, Skillman AG, Warren GL, Ellingson BA, Stahl MT. Conformer generation with OMEGA: Algorithm and validation using high quality structures from the Protein Databank and Cambridge Structural Database. J Chem Inf Model. 2010; 50:572. [PubMed: 20235588]
45. Sanner M, Olsen AJ, Spehner JC. Reduced surface: An efficient way to compute molecular surfaces. Biopolymers. 1996; 38:305–320. [PubMed: 8906967]
46. Hiser C, Mills DA, Schall M, Ferguson-Miller S. C-terminal truncation and histidine-tagging of cytochrome *c* oxidase subunit II reveals the native processing site, shows involvement of the C-terminus in cytochrome *c* binding, and improves the assay for proton pumping. Biochemistry. 2001; 40:1606–1615. [PubMed: 11327819]
47. Qin L, Sharpe MA, Garavito RM, Ferguson-Miller S. Conserved lipid-binding sites in membrane proteins: A focus on cytochrome *c* oxidase. Curr Opin Struct Biol. 2007; 17:444–450. [PubMed: 17719219]
48. Althoff T, Deryck JM, Popot JL, Kühlbrandt W. Arrangement of electron transport chain components in bovine mitochondrial supercomplex I1III2IV1. EMBO J. 2011; 30:4652–4664. [PubMed: 21909073]
49. Beis I, Newsholme EA. The contents of adenine nucleotides, phosphagens and some glycolytic intermediates in resting muscles from vertebrates and invertebrates. Biochemistry. 1975; 152:23–32.
50. Napiwotzki J, Shinzawa-Itoh K, Yoshikawa S, Kadenbach B. ATP and ADP bind to cytochrome *c* oxidase and regulate its activity. Biol Chem. 1997; 378:1013–1021. [PubMed: 9348111]
51. Frank V, Kadenbach B. Regulation of the H+/e(−) stoichiometry of cytochrome *c* oxidase from bovine heart by intramitochondrial ATP/ADP ratios. FEBS Lett. 1996; 382:121–124. [PubMed: 8612732]

52. Buhrow, Leann. PhD thesis. Michigan State University; 2012. Computational prediction and experimental validation of cytochrome c oxidase main-chain flexibility and allosteric regulation of the K-pathway; p. 3549123
53. Follmann K, Arnold S, Ferguson-Miller S, Kadenbach B. Cytochrome *c* oxidase from eucaryotes but not from procaryotes is allosterically inhibited by ATP. Biochem Mol Biol Int. 1998; 45:1047–1055. [PubMed: 9739469]
54. Goglia F, Lanni A, Horst C, Moreno M, Thoma R. In vitro binding of 3,5-di-iodo-L-thyronine to rat liver mitochondria. J Mol Endocrinol. 1994; 13:275–282. [PubMed: 7893345]
55. Simon N, Jolliet P, Morin C, Zini R, Urien S, Tillement JP. Glucocorticoids decrease cytochrome *c* oxidase activity of isolated rat kidney mitochondria. FEBS Lett. 1998; 435:25–28. [PubMed: 9755852]
56. Vaz AR, Delgado-Esteban M, Brito MA, Bolanos JP, Brites D, Almeida A. Bilirubin selectively inhibits cytochrome c oxidase activity and induces apoptosis in immature cortical neurons: assessment of the protective effects of glycoursodeoxycholic acid. J Neurochem. 2010; 112:56–65. [PubMed: 19818102]
57. Malik SG, Irwanto KA, Ostrow JD, Tiribelli C. Effect of bilirubin on cytochrome c oxidase activity of mitochondria from mouse brain and liver. BMC Res Notes. 2010; 3:162–167. [PubMed: 20534120]
58. Moreno M, Lanni A, Lombardi A, Goglia F. How the thyroid controls metabolism in the rat: Different roles for triiodothyronine and diiodothyronines. J Physiol. 1997; 505:529–538. [PubMed: 9423191]
59. Lanni A, Moreno M, Cioffi M, Goglia F. Effect of 3,3′-diiodothyronine and 3,5′-di-iodothyronine on rat liver mitochondria. J Endocrinol. 1993; 136:59–64. [PubMed: 8381457]
60. Lanni A, Moreno M, Horst C, Lombardi A, Goglia F. Specific binding sites for 3,3′-diiodo-L-thyronine (3,3′-T2) in rat liver mitochondria. FEBS Lett. 1994; 351:237–240. [PubMed: 8082770]
61. Goglia F, Lanni A, Barth J, Kadenbach B. Interaction of diiodothyronine with isolated cytochrome *c* oxidase. FEBS Lett. 1994; 346:295–298. [PubMed: 8013649]
62. Lanni A, Moreno A, Lombardi A, Goglia F. Rapid stimulation in vitro of rat liver cytochrome oxidase activity by 3,5-diiodol-thyronine and by 3,3′-diiodo-L-thyronine. Mol Cell Endocrinol. 1994; 99:89–94. [PubMed: 8187965]
63. Lowell BB, Spiegelman BM. Towards a molecular understanding of adaptive thermogenesis. Nature. 2000; 404:652–660. [PubMed: 10766252]
64. Noy N. Between death and survival: Retinoic acid in regulation of apoptosis. Annu Rev Nutr. 2010; 30:201–217. [PubMed: 20415582]
65. Zunszain PA, Ghuman J, McDonagh AF, Curry S. Crystallographic analysis of human serum albumin complexed with 4Z,15E-bilirubin-IX alpha. J Mol Biol. 2008; 381:394–406. [PubMed: 18602119]
66. Sharpe MA, Ferguson-Miller S. A chemically explicit model for the mechanism of proton pumping in heme–copper oxidases. J Bioenerg Biomembr. 2008; 40:541–549. [PubMed: 18830692]
67. Bratton MR, Pressler MA, Hosler JP. Suicide inactivation of cytochrome *c* oxidase: Catalytic turnover in the absence of subunit III alters the active site. Biochemistry. 1999; 38:16236–16245. [PubMed: 10587446]
68. Mills DA, Hosler JP. Slow proton transfer through the pathways for pumped protons in cytochrome *c* oxidase induces suicide inactivation of the enzyme. Biochemistry. 2005; 44:4656–4666. [PubMed: 15779892]
69. Koepke J, Olkhova E, Angerer H, Muller H, Peng G, Michel H. High resolution crystal structure of *Paracoccus denitrificans* cytochrome *c* oxidase: New insights into the active site and the proton transfer pathways. Biochim Biophys Acta. 2009; 1787:635–645. [PubMed: 19374884]
70. Qin L, Liu J, Mills DA, Proshlyakov DA, Hiser C, Ferguson-Miller S. Redox-dependent conformational changes in cytochrome suggest a gating mechanism for proton uptake. Biochemistry. 2009; 48:5121–5130. [PubMed: 19397279]
71. Busenlehner LS, Salomonsson L, Brzezinski P, Armstrong RN. Mapping protein dynamics in catalytic intermediates of the redox-driven proton pump cytochrome *c* oxidase. Proc Natl Acad Sci USA. 2006; 103:15398–15403. [PubMed: 17023543]

72. Buhrow L, Ferguson-Miller S, Kuhn LA. From static structure to living protein, Computational analysis of cytochrome *c* oxidase main-chain flexibility. Biophys J. 2012; 102:2158–2166. [PubMed: 22824280]
73. Tiefenbrunn T, Liu W, Chen Y, Katritch V, Stout CD, Fee JA, Cherezov Y. High resolution structure of the *ba*3 cytochrome *c* oxidase from *Thermus thermophilus* in lipid environment. Plos ONE. 2011; 6:e22348–e22348. [PubMed: 21814577]
74. Hemp J, Gennis RB. Diversity of the heme-copper superfamily in archaea: Insights from genomics and structural modeling. Results Probl Cell Differ. 2008; 45:1–31. [PubMed: 18183358]
75. Verkhovsky MI, Morgan JE, Wikstrom M. Oxygen binding and activation: Early steps in the reaction of oxygen with cytochrome *c* oxidase. Biochemistry. 1994; 33:3079–3086. [PubMed: 8130222]
76. Brzezinski P, Gennis RB. Cytochrome *c* oxidase: Exciting progress and remaining mysteries. Bioenerg Biomembr. 2008; 40:521–531.
77. Antonini E, Brunori M, Colosimo A, Greenwood C, Wilson MT. Oxygen "pulsed" cytochrome *c* oxidase: Functional properties and catalytic relevance. Proc Natl Acad Sci USA. 1977; 74:3128–3132. [PubMed: 198771]
78. Brunori M, Colosimo A, Rainoni G, Wilson MT, Antonini E. Functional intermediates of cytochrome oxidase. Role of "pulsed" oxidase in the pre-steady state and steady state reactions of the beef enzyme. J Biol Chem. 1979; 254:10769–10775. [PubMed: 227852]
79. Brudvig GW, Stevens TH, Morse RH, Chan SI. Conformations of oxidized cytochrome *c* oxidase. Biochemistry. 1981; 20:3912–3921. [PubMed: 6268153]
80. Moody AJ, Cooper CE, Rich PR. Characterization of 'fast' and 'slow' forms of bovine heart cytochrome-*c* oxidase. Biochim Biophys Acta. 1991; 1059:189–207. [PubMed: 1653016]
81. Schoonover JR, Palmer G. Reaction of formate with the fast form of cytochrome oxidase: A model for the fast to slow conversion. Biochemistry. 1991; 30:7541–7550. [PubMed: 1649633]
82. Shoji K, Giuffre A, D'Itri E, Hagiwara K, Yamanaka T, Brunori M, Sarti P. The ratio between the fast and slow forms of bovine cytochrome c oxidase is changed by cholate or nucleotides bound to the cholate-binding site close to the cytochrome *a*3:CuB binuclear centre. Cell Mol Life Sci. 2000; 57:1482–1487. [PubMed: 11078025]
83. Roberts VA, Pique ME. Definition of the interaction domain for cytochrome *c* on cytochrome *c* oxidase: III. Prediction of the docked complex by complete, systematic search. J Biol Chem. 1999; 274:38051–38060. [PubMed: 10608874]

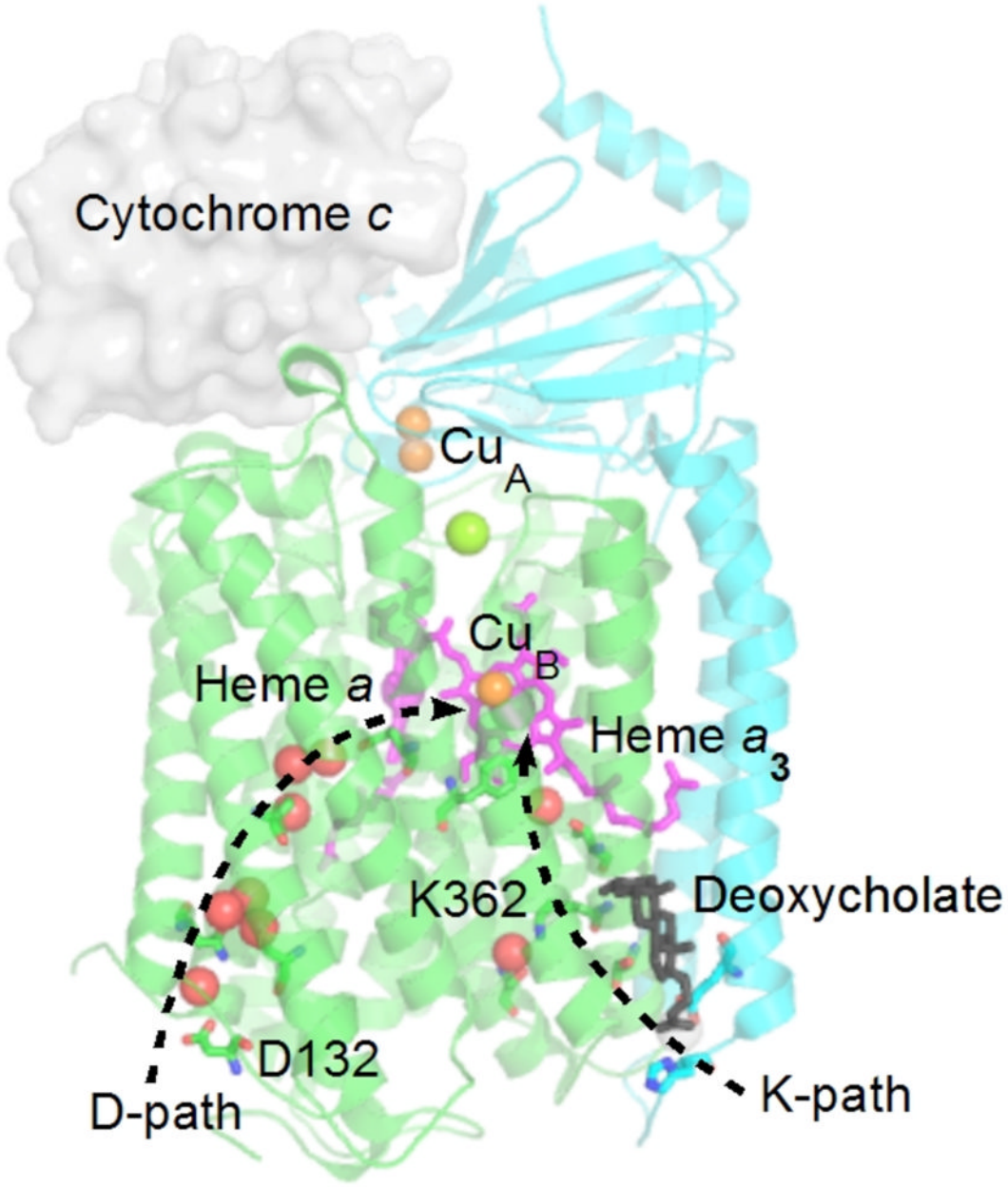

Figure 1. Structure of *R. sphaeroides* cytochrome *c* oxidase

The relative position of the cytochrome *c* substrate is represented by a gray surface, according to the docking analysis of Roberts and Pique, 1999.[83] *Rs*C*c*O (PDB: 3DTU) [31] subunits I and II are depicted as green and cyan ribbons, respectively. Heme (magenta sticks) and copper (copper colored spheres) cofactors, crystallographic deoxycholate (gray sticks), and water molecules (red spheres) are also present. The conserved D- and K-paths for proton uptake are represented as dashed lines leading from the internal side of the membrane to the active site.

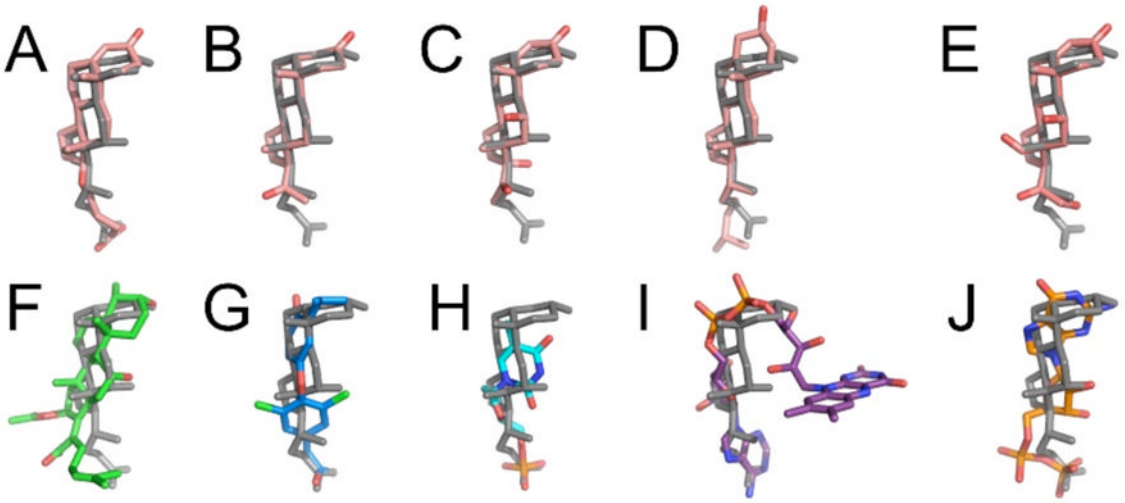

Figure 2. Biological ligands highly similar in shape and chemistry to the C*c*O crystallographic deoxycholate

The *Rs*C*c*O bound DOC and Binding MOAD steroids, retinoic acid, thyroid hormone, nucleotides, and flavins were found to be significantly similar in shape and chemistry as determined by *ROCS*. The top ranked ligands: (A) testosterone hemisuccinate, (B) progesterone, (C) hydrocortisone, (D) cholesterol, (E) aldosterone, (F) fusidic acid, (G) thyroid hormone, (H) retinoic acid, (I) FAD, and (J) GDP are shown as aligned by *ROCS* to the crystallographic DOC (gray sticks).

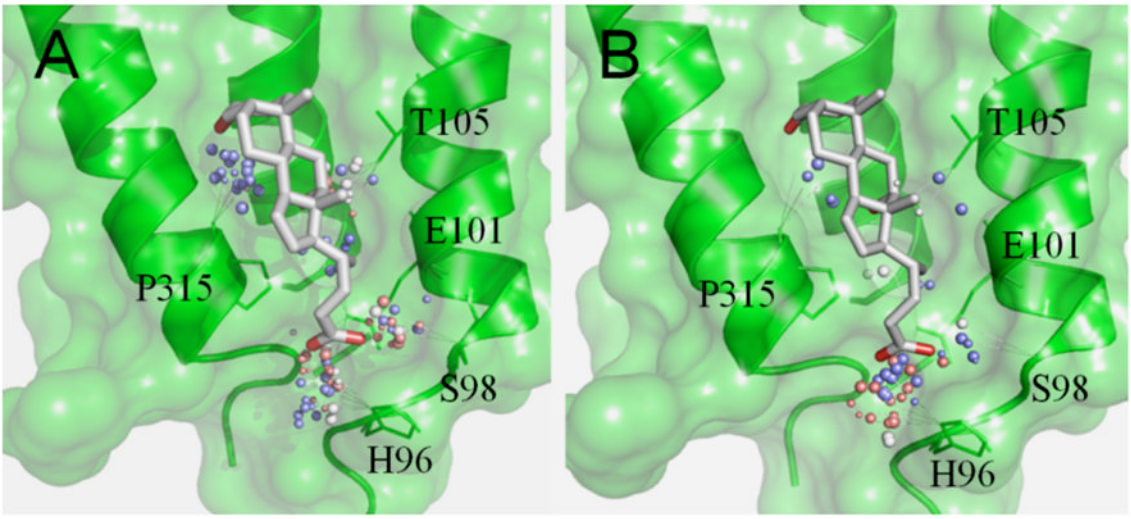

Figure 3. *SimSite3D* points of similar chemistry between the *Rs*C*c*O bile acid binding site and top-scoring ligand site matches from Binding MOAD

(A) Points of chemical interaction in *Rs*C*c*O surrounding subunit I residue P315 and subunit II residues H96, S98, E101, and T105 were frequently matched by nicotinamide, nucleotide, and flavin binding sites. (B) Steroid and lipid binding sites frequently matched the chemistry near *Rs*C*c*O bile acid binding site residue P315 in subunit I and H96 and S98 in subunit II. Small blue and red spheres indicate matched positions for hydrogen-bond donors and acceptors in the top-scoring sites, respectively. White spheres indicate matched hydrogen bond donor and/or acceptor (e.g., hydroxyl group) sites. The crystallographically-defined DOC is shown in light gray sticks.

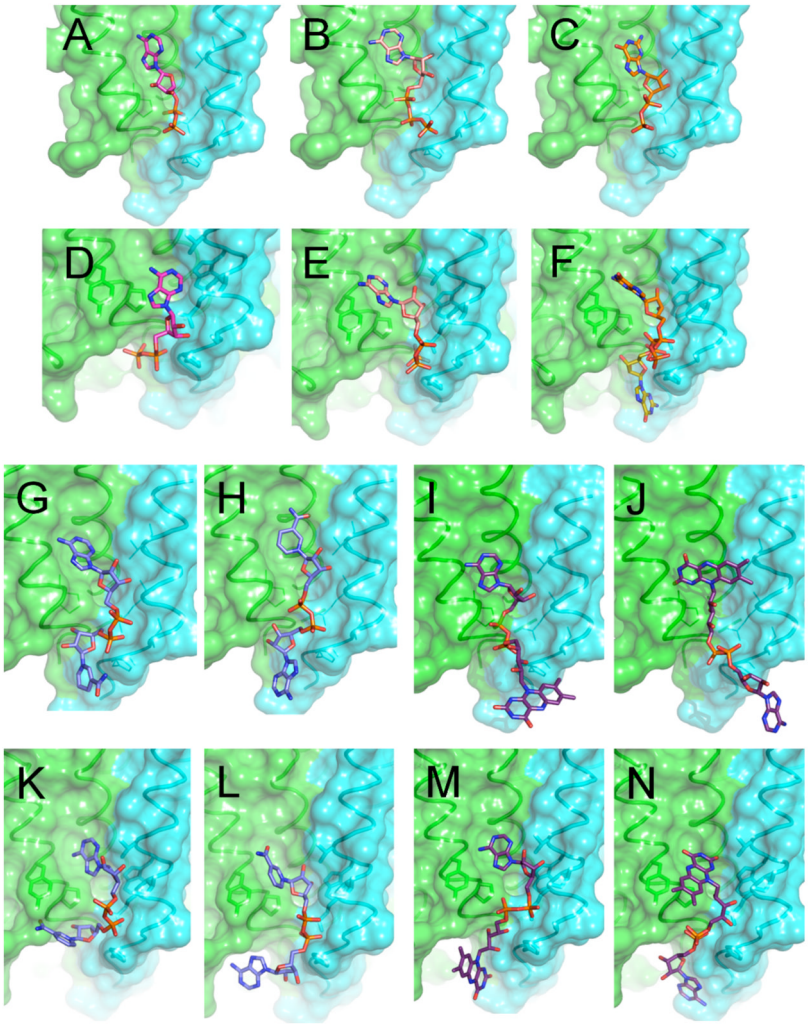

Figure 4. Binding modes predicted by *SimSite3D* site alignment and *SLIDE* docking

For each of the nucleotides, NAD^+, and FAD, *SimSite3D* and *SLIDE* predicted similar binding modes. In all cases, the di- or triphosphate groups are bound near the entrance of the K-path, specifically near H96 and E101. The ribose group was bound in the center of the steroid binding site and interacted with T105. Finally, the nucleic acid base, nicotinamide, or flavin moiety was located furthest into the membrane domain, often interacting near P315. The subunit I (green ribbon)/subunit II (cyan ribbon) interface is depicted with interacting amino acid residues in stick diagram. Binding modes determined by *SimSite3D*: (A) ADP (magenta sticks), (B) ATP (salmon sticks), (C) GDP (orange sticks), (G–H) NAD^+ (blue sticks), and (I–J) FAD (purple sticks). Binding modes determined by *SLIDE* are shown immediately below the *SimSite3D* orientation for the same ligand: (D) ADP (magenta sticks), (E) ATP (salmon sticks), (F) GDP (orange sticks), (K–L) NAD^+ (blue sticks), and (M–N) FAD (purple sticks).

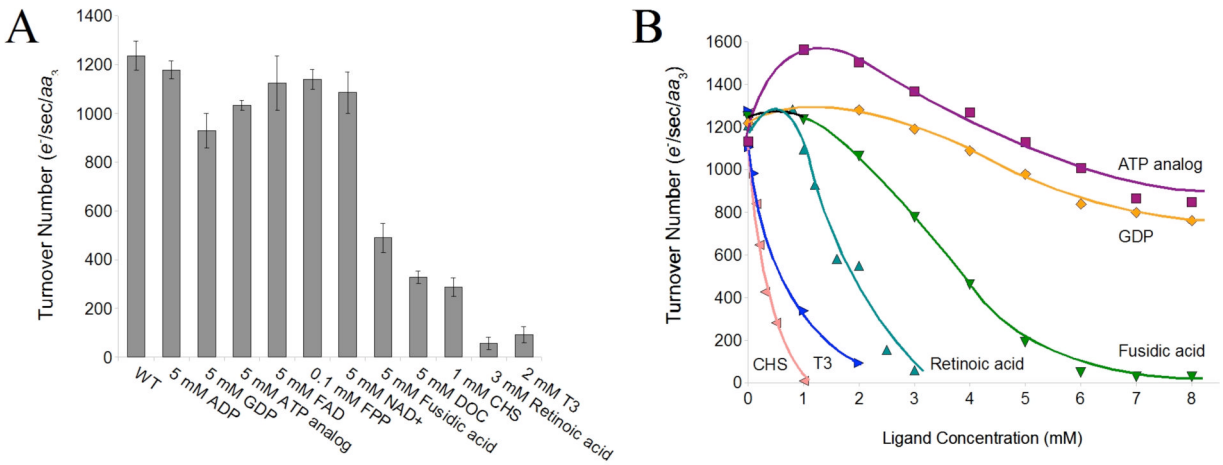

Figure 5. An ATP analog and GDP elicit a low level of *Rs*C*c*O inhibition while fusidic acid, deoxycholate, cholesterol hemisuccinate, retinoic acid, and T3 thyroid hormone inhibit more strongly

(A) The top scoring, commercially available candidate ligands determined by *ROCS* and/ or *SimSite3D* were tested at maximal concentration for their ability to affect *Rs*C*c*O activity with saturating levels of cytochrome *c* substrate. Error bars represent standard deviations from at least three independent trials. (B) Candidate ligands that altered *Rs*C*c*O activity were further investigated under varying ligand concentrations. Assay conditions: 100 mM HEPES pH 7.4, 24 mM KCl, 2.8 mM ascorbate, 1 mM N,N,N′,N′-tetramethyl-p-phenylenediamine (TMPD), 5.6 μM EDTA, 0.01% lauryl maltoside (LM), with 30 μM cytochrome *c* as the substrate.

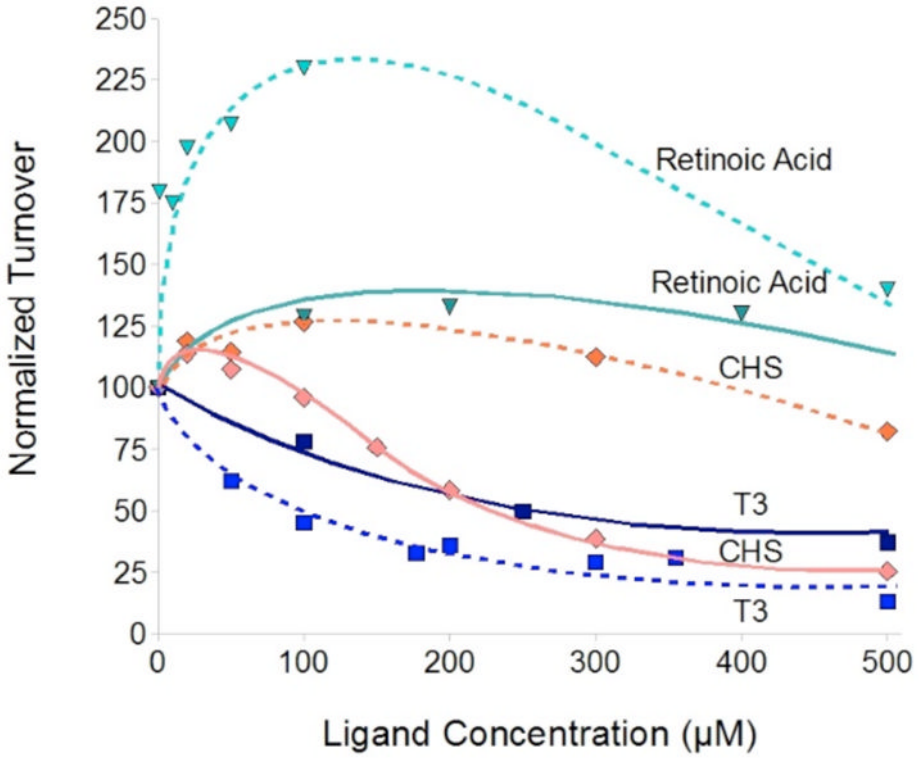

Figure 6. Inhibitory ligands differentially affect the *Rs*C*c*O wild-type and E101A mutant

Ligand effects are determined at saturating levels of cytochrome *c* in both the WT (—) and E101A (- - -) systems. These effects are normalized as compared to protein activity in the absence of a ligand, approximately 1200 e^-/s/aa_3 for WT and 600 e^-/s/aa_3 for the E101A mutant. Retinoic acid (▼) is shown in cyan, CHS (◆) in salmon, and T3 thyroid hormone (■) in blue. Each ligand had a significantly different influence on E101A as compared to WT, consistent with the ligands' influence being due to binding at the bile acid site. Assay conditions as in Figure 5.

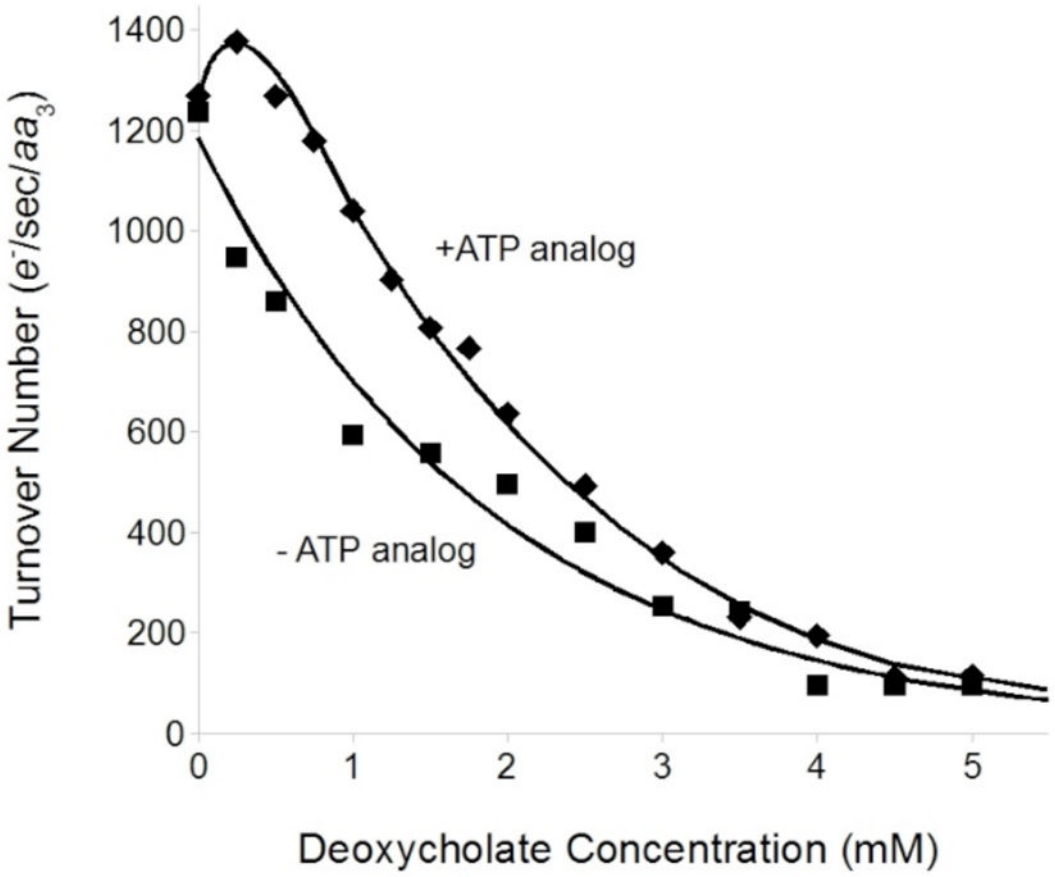

Figure 7. Nucleotides bind to the *Rs*C*c*O bile acid site

The ability of the crystallographically-defined DOC ligand to inhibit activity was monitored at saturating levels of cytochrome *c* in the presence and absence of the ATP analog. This analog, at 5 mM concentration, prevented DOC from inhibiting *Rs*C*c*O activity, presumably because of its ability to compete at the bile acid site. Assay conditions as in Figure 5.

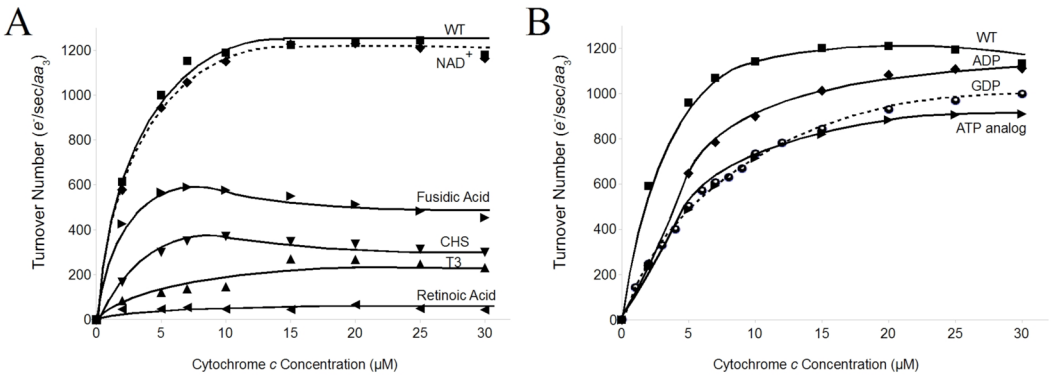

Figure 8. Nucleotides inhibit *Rs*C*c*O under low substrate conditions while fusidic acid, retinoic acid, cholesteryl hemisucinate, and T3 thyroid hormone strongly inhibit activity at all substrate concentrations

Physiological concentrations of all ligands, except for the fusidic acid antibiotic, were tested for their ability to affect *Rs*C*c*O activity under varying concentrations of cytochrome *c* substrate. (A) Five mM fusidic acid, 250 μM cholesteryl hemisuccinate, 500 μM T3 thyroid hormone, and 1.5 mM retinoic acid ligands strongly inhibit activity in all concentrations of cytochrome *c*. Nicotinamides did not affect enzyme activity. (B) Under low cytochrome *c* conditions, 5 mM ADP, ATP analog, or GDP inhibited the enzyme with sigmoidal behavior, consistent with ATP inhibition of bovC*c*O. Assay conditions as in Figure 5, with 0 – 30 μM cytochrome *c*.

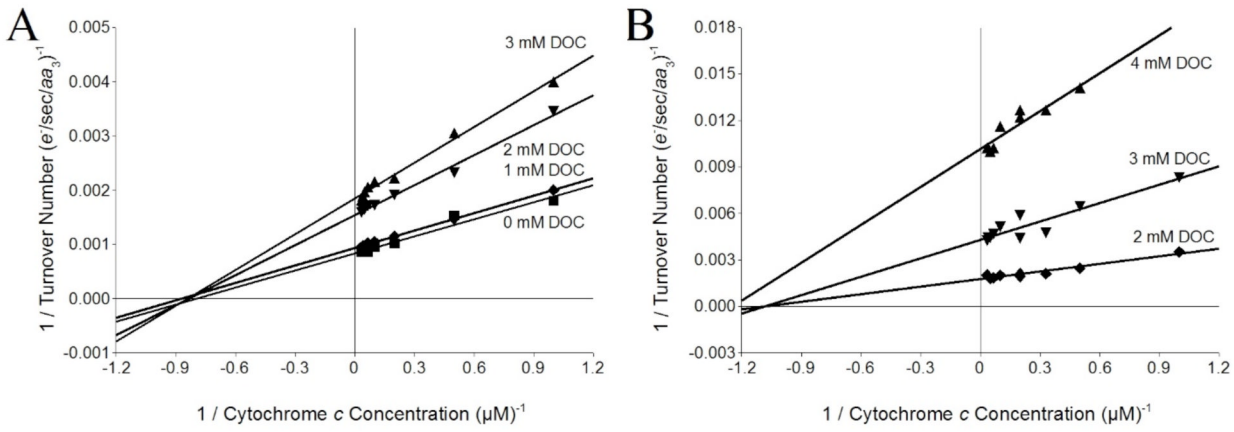

Figure 9. Deoxycholate noncompetitively inhibits the *Rs*C*c*O WT and E101A mutant

The double reciprocal plots of activity versus non-saturating substrate concentration (0–30 μM) are consistent with the noncompetitive inhibition of the *Rs*C*c*O (A) WT and (B) E101A mutant. The K_m of cytochrome *c*, ~1 μM, is unchanged by the DOC inhibition. Assay conditions as in Figure 5, with 0–30 μM cytochrome *c*.

Table 1
Predicted ligand candidate chemical classes

The first panel lists *ROCS*-analyzed ligands scoring at least three standard deviations above the average TanimotoCombo score across Binding MOAD (≥ 0.85; where more positive scores indicate greater ligand similarity). The second panel lists *SimSite3D* protein binding site matches scoring at least two standard deviations below the average *SimSite3D* score across Binding MOAD (≤ −2.00; where more negative scores indicate greater site similarity). The ligands and binding sites were grouped into dominant chemical classes and redundant ligands or protein binding sites were removed.

Method	Ligand Class	Number of Ligands in Top Scoring Results	Average Tanimoto Combo Score
ROCS	Bile acids	10	1.17
	Steroids	31	0.96
	Retinoic acid analogs	5	0.94
	Amino acid analogs	8	0.91
	Nucleotide and flavin analogs	6	0.9
	Thyroid hormone analogs	2	0.87
			Average *SimSite3D* Score
SimSite3D	Nicotinamides	55	−2.43
	Flavins	24	−2.31
	Lipids	21	−2.27
	Nucleotides	44	−2.24
	Steroids	5	−2.07

Table 2

***SLIDE* docked ligands and their protein interactions**

SLIDE was used to dock riboside candidate ligands into the *Rs*C*c*O steroid binding site. The top scoring binding orientations were characterized as scoring two standard deviations or better than the average *SLIDE* OrientScore for an individual molecule. These top scoring dockings were divided based on whether the bound ligand fragment was a nucleic acid base, flavin moiety, or neither. The percentage of ligands interacting with the eight most frequently contacted *Rs*C*c*O residues is listed.

Ligand	Interacting Fragment	Orient- Score	Affi- Score	Percentage of docked ligand interactions							
				Subunit I				Subunit II			
				P315	Y318	H96	S98	E101	I102	W104	T105
ADP	Adenine	−8.0	−7.0	100	33	100	100	100	100	33	10
ATP	Adenine	−8.7	−7.9	88	77	100	88	100	85	62	77
GDP	Guanine	−8.1	−7.1	90	90	90	40	80	50	80	60
GDP	None	−8.1	−7.5	100	14	100	71	79	0	0	7
FAD	Adenine	−9.7	−10	83	50	83	83	100	67	0	67
FAD	Flavin	−9.2	−9.9	100	82	91	64	100	64	41	55
NAD^+	Adenine	−9.3	−8.6	100	54	100	87	97	79	36	90

Table 3

Percentage of protein binding site matches between the C*c*O steroid binding site and diverse Binding MOAD sites

SimSite3D aligns ligand binding sites based on the site's chemically labeled template points and the solvent-accessible molecular surface. The aligned points between the C*c*O bile acid site and diverse proteins in Binding MOAD may then be mapped back to individual residues. Five C*c*O residues were identified as being shared by high-scoring, diverse sites. The percentage of sites sharing a given residue interaction is shown below.

C*c*O residue	Nucleotide sites	Nicotinamide sites	Flavin sites	Steroid sites	Lipidic sites
P315	52	63	87	60	36
H96	70	91	100	60	100
S98	54	67	65	60	29
E101	66	100	50	0	29
T105	96	100	65	20	19